Nonorthogonal tight-binding model for germanium

N. Bernstein, M. J. Mehl, and D. A. Papaconstantopoulos
Center for Computational Materials Science, Naval Research Laboratory, Washington, DC 20375
(Received 18 December 2001; revised manuscript received 25 February 2002; published 30 August 2002)

We present a pair of nonorthogonal tight-binding (TB) models for germanium within the NRL-TB approach. One uses an sp^3 basis, and is optimized for total-energy calculations by fitting to the total energy and band structures of several high-symmetry lattice structures. The other uses an sp^3d^5 basis to accurately reproduce the diamond lattice band structure, including three conduction bands. We present tests of the sp^3 TB model on bulk properties, including high-symmetry lattice structure energies and volumes and the diamond lattice elastic constants, phonons, and band structure. We also present results for point defect formation and relaxation energies and low index surface energies and stresses, many of which have not been calculated using the density-functional theory (DFT), as well as some medium size clusters. Taking advantage of the computational efficiency of the TB approach, we go beyond the capabilities of standard density-functional theory, combining it with molecular dynamics to simulate finite temperature properties of Ge. We get good agreement with experiment for the atomic mean-squared displacement and the melting point approximated using the Lindemann criterion, as well as the linear thermal-expansion coefficient. In another demonstration of the efficiency of the TB approach, we present results for the structure and electronic properties of a high angle twist grain boundary (GB). In agreement with DFT simulation we see a range of structures with comparable energies, all with electronic states deep in the band gap. In contrast to previous work we find some different geometries with perfect fourfold coordination of all atoms in the GB. Despite the perfect coordination, these structures also have deep electronic states in the gap, indicating that the GB will be electrically active.

DOI: 10.1103/PhysRevB.66.075212 PACS number(s): 71.15.Nc, 71.15.Pd, 71.20.Mq, 61.72.Mm

I. INTRODUCTION

The tight-binding (TB) approach to total-energy calculation is one of the simplest methods that explicitly treats the quantum-mechanical nature of electrons that form interatomic bonds. It is much faster than the first-principles approaches, while keeping enough of the essential physics to be more reliable than the empirical interatomic potentials. TB methods have been developed for a wide range of materials, from metals to semiconductors.[1] While most of the work on models for semiconductors has concentrated on silicon and carbon, there has been less development of TB total-energy models for germanium.[2–6] There are a number of models that focus entirely on the band structure,[7–10] and several aimed at the energetics of small clusters. Thus far there has been relatively little emphasis, both in the fitting data and the published results, on bulk energetics beyond a few simple tests of high-symmetry bulk phases and phonon frequencies. In this work we present a pair of nonorthogonal TB models for Ge using the formalism of the NRL-TB method.[11,12] The first model uses an sp^3 basis, and is optimized for total-energy calculations. All of the results we present that require total energy or atomic force or stress calculations are done using this TB model. We present tests of this model on bulk phase energetics, elastic and vibrational properties, point defects energies and structures, low index surface properties, and cluster energies and structures. We have tested the effects of charge self-consistency (CSC) on this model using a method based on a recent formulation for including CSC in the TB approach.[13] While we find no significant changes to any of the bulk or point defect results, the surface properties are modified considerably. The second model uses an sp^3d^5 basis that is needed to accurately represent the band structure to which it is fitted, including the valence bands and the lowest few conduction bands. While this model could also be used for total-energy calculations, doing so would be much more computationally expensive than with the sp^3 basis model, and the energies, which depend only on occupied orbitals with little d character, would not be significantly improved. Therefore for the sp^3d^5 basis model we only present the band structure, and only band structure related results are computed using this model.

The TB formulation uses parametrized relations to describe the electronic Hamiltonian and overlap matrices. In the NRL-TB formulation used for this TB model, the parameters are determined by fitting a combination of band structures and energies to first-principles calculations. The TB approach is more computationally economical than first-principles approaches both because it uses a much smaller basis and because it makes various approximations as to the nature of the Hamiltonian matrix that characterizes the electrons. In addition, because the TB approach uses localized orbitals, it is also more amenable for use with linear-scaling methods for computing energies and forces than typical first-principles methods. While it is much faster than first-principles approaches, the TB method is still significantly more computationally demanding than methods using empirical interatomic potentials. However, it is more reliable than the non-quantum-mechanical methods, especially far from equilibrium or far from the geometries that were used in the fit. In addition, it is easier to include electron CSC effects in TB methods, and unlike any method that does not explicitly treat the electrons, TB methods can provide electronic structure information as well as total energies and forces.

In Sec. II we discuss the functional form of the expres-

sions that contribute to the model, and the database of first-principles calculations used in the fit. In Secs. III, IV, V, and VI we present zero-temperature results for bulk, point defect, surface properties, and clusters, respectively, and in Sec. VII we present results for some finite temperature properties. We discuss results of our application of these models to the structural and electronic properties of a high angle twist grain boundary in Sec. VIII, and in the final section we give some concluding remarks.

II. FUNCTIONAL FORM AND FITTING

The TB model we present uses the NRL-TB framework previously used for silicon.[12] In this approach, the electronic energy is defined as a sum over occupied eigenvalues that are the solution to a generalized eigenvalue problem. The Hamiltonian (H) and overlap (S) matrices are written in an sp^3 or sp^3d^5 basis centered around each atom. The off-diagonal H and S matrix elements are defined in the two-center approximation, i.e., they are dependent only on the relative positions of the two interacting atoms. The diagonal H matrix elements are written as a function of the local atomic density that is dependent on the distances from the atom to its neighbors. This creates an explicit environment dependence in the diagonal matrix elements.

The functions describing the distance dependence of the off-diagonal S and H matrix elements, as well as the diagonal H matrix elements, are parametrized in the same way as our previous work on Si,[12,14] using 41 parameters. These parameters are used to fit the sp^3 model to the total energies and band structures of a number of bulk structures: diamond (DIA), simple cubic (sc), body-centered cubic (bcc), face-centered cubic (fcc), and the diamond structure with a distortion corresponding to the Raman phonon. To create the fitting data each structure is simulated at a range of atomic volumes, about 13.5–24.0 Å^3 for the DIA structure and about 15–21 Å^3 for the other three structures. At each volume the full-potential linearized augmented plane-wave method (FPLAPW) is used to compute energies and the muffin-tin augmented plane-wave method (MTAPW) is used to compute band structures.[15–18]

Generating our LAPW database we were presented with the well-known problem that scalar relativistic calculations do not give an energy gap in Ge. The state $\Gamma_{2'}$ switches with the $\Gamma_{25'}$ and closes the gap completely at the Γ point. It has been shown[19] that a nonrelativistic calculation pushes the $\Gamma_{2'}$ state upward and creates a small gap of 0.26 eV. To create a robust TB parametrization we use the band structures from the nonrelativistic calculations, but use the more accurate scalar relativistic FPLAPW total-energy values. Furthermore, conduction bands are then shifted rigidly to approximately match the band gap, which is underestimated by the local-density approximation (LDA) to density-functional theory (DFT), to the experimental value.[20,21] One of the features of the NRL-TB method is that the TB model is fitted to first-principles band structures that contain all of the information needed to compute the total energy. This is done by shifting the first-principles eigenspectrum by an appropriately normalized quantity related to the density-functional theory double-counting terms.[11,22,23] The TB model energy is fitted to the FPLAPW total energy, and the TB model eigenvalues are fitted to the shifted MTAPW band structure for the diamond lattice. The sp^3d^5 model is fitted using 69 parameters to the band structure of the diamond lattice at nine volumes ranging from 19.7 Å^3 to 24.0 Å^3.

To improve the band-structure fit of both the sp^3 and sp^3d^5 models some symmetry information is used at two high-symmetry points in the Brillouin zone (BZ) of the diamond lattice, the Γ and L points. At these two k points the matrix is block diagonalized into bands with appropriate symmetries and degeneracies, four eigenvalues at the Γ point and five eigenvalues at the L point. This allows us to fit each TB model band to the appropriate APW band, rather than just assuming that the ordering of the TB bands is the same as the APW ordering. In fact, our experience is that for many otherwise reasonable TB model parameter sets this is not the case. The parameters resulting from the fit, in the same notation as Ref. 12, are listed in Tables I and II.[24]

The CSC effects discussed in Sec. V are included through an approach quite similar to the work of Elstner *et al.*[13] The total energy is written as an eigenvalue sum plus an electrostatic contribution, computed by assigning a charge to each atomic site using a Mulliken population analysis. The resulting expression for the total energy is

$$E^{TB}=\sum_{i}^{N} f(\epsilon_i)\epsilon_i+\frac{1}{2}\sum_{\alpha\beta}^{N_A}\gamma_{\alpha\beta}\Delta q_\alpha \Delta q_\beta . \tag{1}$$

As in Eq. (19) of Ref. 13, N is the number of basis elements, ϵ_i is the eigenvalue of state i, $f(\epsilon)$ is the Fermi function, N_A is the number of atoms, Δq_α is the local charge at atom α, and $\gamma_{\alpha\beta}$ gives the Coulomb interaction between charges on atoms α and β. In our work the net charge (the Mulliken charge minus the nuclear core charge) is assumed to be spread out in a Gaussian charge-density profile in contrast to the exponentially decaying charge density used in Ref. 13. Using the work of Shavitt,[25] it can be shown that the width of the charge distribution is determined by its onsite Coulomb energy U_α so that the normalized charge distribution is

$$\rho_\alpha(r)=\left(\frac{U_\alpha^2}{2}\right)^{3/2}\exp\left(-\frac{\pi}{2}U_\alpha^2 r\right). \tag{2}$$

This gives the matrix $\gamma_{\alpha\beta}$ a different functional form as a function of distance between atoms α and β than in Eq. (17) of Ref. 13. After significant simplification of the expressions tabulated by Shavitt,[25] the resulting value for $\gamma_{\alpha\beta}$ is

$$\gamma_{\alpha\beta}=\sum_{\beta'}\frac{1}{R_{\alpha\beta'}}+U_\alpha\delta_{\alpha\beta}-\sum_{\beta'}\left[\frac{1}{R_{\alpha\beta'}}-\frac{1}{R_{\alpha\beta'}}\,\mathrm{erf}\left(\sqrt{\frac{\pi}{2}\left(\frac{U_\alpha^2U_\beta^2}{U_\alpha^2+U_\beta^2}\right)}R_{\alpha\beta'}\right)\right], \tag{3}$$

where $R_{\alpha\beta'}$ is the distance from atom α to the periodic image of atom β, and the sums are carried out over all of the periodic images of atom β except where $R_{\alpha\beta'}$ is zero. The

TABLE I. Parameters for Ge sp^3 basis nonorthogonal tight-binding model.

		Onsite parameters		
λ	1.1563			
Orbital	α (Ry)	β (Ry)	γ (Ry)	χ (Ry)
s	−0.1651	0.4169	−94.7331	1317.1121
p	0.2001	8.8689	−132.9293	470.2755
		Hamiltonian matrix parameters		
Interaction	a (Ry)	b (Ry/a.u.)	c (Ry/a.u.^{2})	g (a.u.$^{-1/2}$)
$H_{ss\sigma}$	583.7307	−111.8091	−22.9811	1.3251
$H_{sp\sigma}$	12.5370	−5.6445	0.4230	0.8631
$H_{pp\sigma}$	−19.7343	2.1006	1.4542	1.0073
$H_{pp\pi}$	2004.8465	−1054.6059	137.1944	1.3847
		Overlap matrix parameters		
Interaction	t (a.u.$^{-1}$)	q (a.u.$^{-2}$)	r (a.u.$^{-3}$)	u (a.u.$^{-1/2}$)
$S_{ss\sigma}$	−0.7513	0.4634	−0.0503	0.8028
$S_{sp\sigma}$	−2.0975	1.5437	−0.1781	0.9118
$S_{pp\sigma}$	−25.5413	14.0312	−1.8615	1.0599
$S_{pp\pi}$	−1.2532	0.8381	−0.0812	0.8325

first sum is evaluated using an Ewald technique,[26] while the second sum is short ranged and can be evaluated by explicit summation.

The electrostatic term in the total energy leads to a modification of the eigenvalue equation that depends on the electronic occupation. We solve the resulting self-consistent eigenvalue problem using the modified Broyden method of Johnson.[27] Since the structures used in the fit of the parameters are all high-symmetry lattices, they will, by construction, have no contribution from the CSC terms. Therefore, the addition of these terms will not affect the computed properties of any of the structures used in the fit or the best-fit set of parameters.

III. BULK PROPERTIES

We begin by presenting the results of our TB models for properties of bulk phases of Ge. Some of these properties were included in the fit, specifically the band structure and the total energy of the DIA structure, and the energies of the sc, fcc, and bcc structures as well as the Raman phonon frequency. We also compute the energies and equilibrium volumes of a number of additional low-energy structures for Ge not included in the fit, as well as phonon frequencies at some high-symmetry points, and the elastic properties of the diamond structure. The high degree of symmetry of all of these structures means that none will be affected by the CSC terms, and so these are not used in any of the calculations discussed in this section.

The band structures computed with the sp^3 and sp^3d^5 TB models are plotted in Fig. 1, together with the scissor-shifted MTAPW band structure for comparison. The fit of the sp^3 model for the valence band, which contributes to the total energy, is very good. The fit for the conduction band, while qualitatively reasonable at least for the lowest two bands, is less accurate. Instead of an indirect gap of 0.70 eV (the scissor-shifted MTAPW value) from the valence-band Γ maximum to the conduction-band L minimum and a direct gap of 0.86 eV at Γ, the TB model has an indirect band gap of 0.36 eV from the Γ point to the L point, while the direct gap at Γ is 0.94 eV. The description of the conduction band in the sp^3d^5 model is better, particularly at the X and W points, but also in the quantitative value of the band gap. In this model, which was designed for band-structure related studies, there is an indirect gap from Γ to L of 0.67 eV, in very good agreement with the scissor-shifted MTAPW value, and a direct gap at Γ of 1.07 eV, a small but significant overestimate. In addition, the sp^3d^5 model gives a good representation of the lowest three conduction bands fitted. Higher conduction bands cannot be treated by this model because a one-to-one correspondence with MTAPW results would require an additional s basis orbital. The corresponding densities of states, including the decomposition into s, p, and d contributions are plotted in Fig. 2. The total densities of states are in good agreement up to about 7 eV above the valence-band maximum, consistent with the good band-structure fit. In addition, the decomposition into s, p, and d contributions, which contains information about the eigenvectors that was not fitted, is in very good agreement in the valence band, although the contribution from d orbitals in the bottom of the conduction band is underestimated by the TB model.

The total energies as a function of volume for the bulk structures used in the fit are plotted in Fig. 3 together with the LAPW results to which they were fitted. It is clear from the plot that the total-energy fit for these structures is good. The equilibrium total energies and structures for a number of bulk phases were computed by minimizing the total energy with respect to unit-cell size and shape, and with respect to the internal degrees of freedom. The energy, volume, and unit-cell structural parameters are listed in Table III. For the phases that were in the fit (marked with an asterisk in the table), the agreement is quite good. For the most important

TABLE II. Parameters for Ge sp^3d^5 basis nonorthogonal tight-binding model.

Onsite parameters				
λ	1.1460			
Orbital	α (Ry)	β (Ry)	γ (Ry)	χ (Ry)
s	−0.1521	0.4024	−98.4027	1216.2967
p	0.1771	8.4931	−135.2850	586.5797
d	0.7974	10.3844	191.6903	−499.8657
Hamiltonian matrix parameters				
Interaction	a (Ry)	b (Ry/a.u.)	c (Ry/a.u.^{2})	g (a.u.$^{-1/2}$)
$H_{ss\sigma}$	732.7203	−116.8840	−27.6353	1.3212
$H_{sp\sigma}$	12.9676	−5.6016	0.3728	0.8719
$H_{pp\sigma}$	−20.1730	1.8390	1.3691	1.0235
$H_{pp\pi}$	2112.4087	−1045.6335	134.1094	1.3597
$H_{sd\sigma}$	−1.2543	−0.0608	0.0358	0.6912
$H_{pd\sigma}$	−1173.1549	128.9283	39.8097	1.3063
$H_{pd\pi}$	1.6742	0.2284	−0.0246	0.7920
$H_{dd\sigma}$	−1.3554	0.1931	0.0265	0.5823
$H_{dd\pi}$	−3.1321	−0.1873	0.0261	0.6370
$H_{dd\delta}$	−2469.4178	−42.4797	431.5692	1.4323
Overlap matrix parameters				
Interaction	t (a.u.$^{-1}$)	q (a.u.$^{-2}$)	r (a.u.$^{-3}$)	u (a.u.$^{-1/2}$)
$S_{ss\sigma}$	−0.0123	0.4949	−0.0685	0.8978
$S_{sp\sigma}$	−1.8880	1.5813	−0.1682	0.8948
$S_{pp\sigma}$	−28.7778	13.8696	−1.7678	1.0013
$S_{pp\pi}$	−0.9096	0.8928	−0.0903	0.8349
$S_{sd\sigma}$	−6.7339	0.3042	0.1161	1.0784
$S_{pd\sigma}$	0.0393	0.0282	−0.0037	0.4805
$S_{pd\pi}$	0.6969	−0.1259	0.0236	0.8570
$S_{dd\sigma}$	−32.5704	2.3983	1.0705	1.0716
$S_{dd\pi}$	8.3475	−0.4413	−0.9967	1.0940
$S_{dd\delta}$	4.2025	0.6216	−0.1319	1.0207

high-pressure phase, the β-Sn phase, as well as for the simple hexagonal (sh) structure agreement is also good. For the other phases where DFT calculations are available, *h*-DIA, and bc8, agreement is reasonable, and in every case the energy is higher than that for the experimental ground state, the diamond structure. One important note is that there are two very different values in the literature for the body centered 8 atom (bc8) structure minimum energy and relaxed volume. Although the total-energy difference relative to the diamond structure is overestimated by the TB model, it is much closer to the results of Mujica and Needs than to the work of Crain *et al.*[28,29]

The elastic constants of the diamond structure lattice were calculated by applying appropriate deformations to the structure, relaxing with respect to the internal degrees of freedom, and computing the relaxed energy. The energy as a function of deformation was fitted to a quadratic expression to determine the elastic moduli,[30] and the results are listed in Table IV. The elastic constants of the TB model are in reasonable agreement with DFT/LDA calculations, although the shear modulus c_{44} is significantly overestimated. The elastic moduli are moderately sensitive to the unit-cell volume, as can been seen by the softening of the lattice at the experimental volume of 45.08 Å^3/atom. As a test of another aspect of the elasticity of the material we computed the phonon spectrum along the high-symmetry directions of the vibrational Brillouin zone of the diamond lattice using the frozen phonon method.[31] The results, as well as first-principles calculations and experimental measurements, are plotted in Fig. 4. Agreement with experiment and with DFT calculations is again reasonable, comparable to the elastic constants.

IV. POINT DEFECTS

Point defects are one of the major sources of disorder in semiconductors, since they are thermodynamically favored to exist with finite concentration at finite temperature. They mediate diffusion in the solid, since the stiffness of the perfect diamond lattice makes it nearly impossible to diffuse without defects. Point defects can therefore have a significant effect on dopant profiles. We have calculated the energies and structures of several plausible point defects in Ge. These calculations include the vacancy, as well as three self-interstitial positions, the tetrahedral, hexagonal, and $\langle 110 \rangle$ dumbbell interstitials. All the calculations were done in a 216 atom cubic supercell at the equilibrium lattice constant, sampling the Brillouin zone at the Γ point. The ideal defect

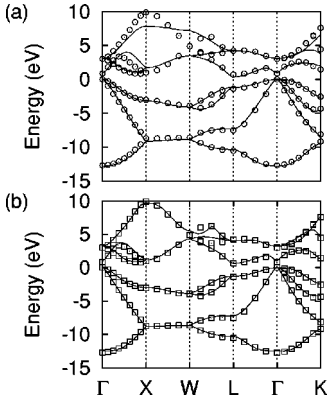

FIG. 1. Four valence and three conduction bands for the diamond lattice using the Ge sp^3 (top panel) and sp^3d^5 (bottom panel) TB models (solid lines) and scissor-shifted MT-APW first-principles calculation (symbols). All energies are computed relative to the valence-band maximum.

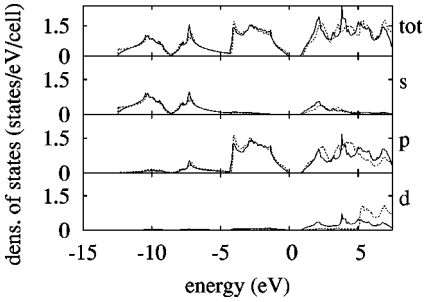

FIG. 2. Electronic densities of state for the diamond lattice. Dashed lines are TB model results, and solid lines are the scissor-shifted nonrelativistic MTAPW results consistent with the fitting database.

geometries were perturbed slightly by randomly displacing each atom, and relaxed using a conjugate-gradient algorithm. The ideal and relaxed formation energies of the defects are listed in Table V. Despite the relatively low symmetry of the point defect geometries and the presence of inequivalent atoms, we found only negligible effects from the inclusion of CSC. Presumably the insensitivity of the calculation to CSC is due to the low level of charge transfer even in the noninteracting electron calculation. Since no formation or relaxation energy changed by more than 0.1 eV, we do not include the CSC terms in any of the results presented in this section.

For the most part the relaxed point defects keep the symmetry of the unrelaxed defects. The atoms neighboring the vacancy relax inward, reducing their distances from 3.95 Å to 3.48 Å. The tetrahedral interstitial makes two 2.42-Å bonds and two 2.50-Å bonds, only slightly deviating from its initial symmetry. The hexagonal interstitial maintains six bonds of length 2.50 Å. The $\langle 110 \rangle$ interstitial, analyzed in detail in Ref. 32, has a structure similar to that of the DFT/LDA simulation. The dumbbell atoms form 2.59-Å bonds with their noninterstitial neighbors, quite close to the DFT/LDA result. The main difference is that the intradumbbell bond is 2.49 Å in the TB model result, significantly shorter than the 2.60 Å found in the DFT/LDA work. The relatively high symmetry of three of the structures (the vacancy, tetrahedral and hexagonal interstitials) is quite different from the results for the NRL-TB model for Si. This shows the emergence of reduced directionality and increased tendency to metal-like properties for Ge as compared with Si.

V. SURFACES

Semiconductor surfaces govern the deposition and growth properties of these technologically important materials. The geometries present at surfaces, characterized by lower coordination and significant bond-angle distortions relative to the bulk, are quite different from the structures used to fit the TB model. As a more stringent test of the transferability of the model, we compute the surface energies and stresses for some low-energy reconstructions of the (111), (100), and (110) surfaces of Ge. The results are summarized in Table VI. The effects of CSC on the surface properties, which are quite large in some cases, are discussed below.

There are only a few first-principles calculations of Ge surface energies and stresses,[33–37] and it is difficult to obtain reliable experimental data for these properties. For the geometries and reconstructions where first-principles calculations have been published, the TB model is in reasonable agreement. Qualitative aspects, including the energy ordering of (100) vs (111), and at least the sign and magnitude of the surface stress for the (111) clean and T_4 adatom covered reconstructions, are all reproduced by the TB model. The quantitative agreement is not as good, with the TB model underestimating the energy gain upon dimerization of the (100) surface, and overestimating the energy gain for buckling of the dimers. While no specific comparison has been made for Ge, surface properties, particularly surface stresses, have been a problem for empirical interatomic potentials for other semiconductors such as silicon.[38] It is reassuring that our TB model, despite having been fitted to a rather different set of geometries, is transferable to the low coordination and large bond distortions present at the surface.

While almost all of the surface energies and stresses we computed are of comparable magnitude to DFT/LDA calculations and to each other, the (110) surface stress stands out. In addition, the structure of the (110) surface is quite unusual: the bonds connecting the surface atoms to the subsurface layer are 2.74 Å long, as compared with a bond length of 2.43 Å in the bulk. Such long bonds are not seen in any other surface structure, nor have they been seen in any first principles or experimental study of semiconductor surfaces that we are aware of. One likely reason for the behavior of the TB model is the neglect of charge-charge interactions. Since the surface atoms are in a very different environment that even the first subsurface layer, significant charge transfer to or from surface states could dramatically change the interatomic bonding. The changes in the surface energies, stresses, and structures due to the inclusion of CSC terms in the calculation allow us to gauge the extent of such charge-transfer effects.

A comparison of the TB and TB-CSC values in Table VI shows that the importance of charge-transfer effects varies greatly between the different properties and structures. The

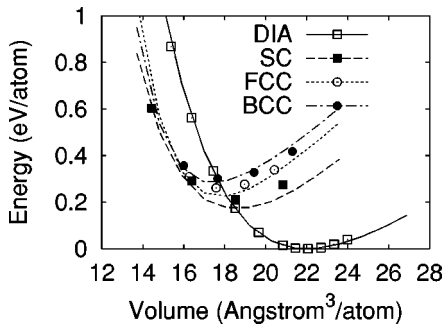

FIG. 3. Total energy as a function of volume for bulk lattice structures included in the fit. Lines are TB model results, and symbols are LAPW results from the fitting database.

(111) surface is almost entirely unaffected, as is energy and stress of the 2×1 buckled dimer reconstruction of the (100) surface. However, the structure of the surface dimer is in slightly better agreement with DFT/LDA results than the conventional TB results. The (100) 2×1 flat dimer reconstruction energy is in much better agreement with DFT/LDA, and the surface stress changes significantly, although no comparison value is available for the latter quantity. The most significant changes take place on the (110) surface, where the energy goes up by 15% and the stress drops by an order of magnitude. The bonds connecting the surface atoms to the subsurface layers are now only 2.41 Å long, slightly shorter than the bulk bond length. While we are not aware of any DFT/LDA or experimental data to compare to, the surface stress and bond lengths from the CSC calculation are much more plausible than the non-CSC results.

VI. CLUSTERS

One interesting class of Ge structures that is most different from the fitting regime of the TB model is small clusters. Up to a few tens of atoms the majority of the material is on the surface, with no bulk-like region at all. To test the transferability of the sp^3 TB model we used it to search for low-energy structures of Ge clusters, starting from the two atom dimer to a 10 atom cluster. Since there are essentially no symmetry constraints on cluster geometries, an exhaustive search for the ground-state structure for clusters beyond a few atoms is quite involved. Since we are mainly interested in benchmarking the performance of the TB model, we only tested structures that have previously been proposed for Ge clusters. We find that for up to six atoms the TB model makes significant errors, indicating that this size regime is outside of the range of validity of the present parametrization. In particular, the range of local atomic densities, which directly affects the on-site matrix elements, is significantly lower than for the bulk geometries in the fitting database. This could probably be remedied by a reparametrization with a fitting database that concentrated on cluster properties. For clusters of seven to ten atoms, the results of the model are

TABLE IV. Elastic constants (in GPa) for the diamond structure computed with the TB model at the equilibrium volume $V_{\rm eq}$, the TB model at the experimental volume $V_{\rm exp}$, plane-wave pseudopotential DFT/LDA calculations (Ref. 59) our LAPW DFT/LDA calculations at V_{eq}, and experiment (Refs. 60,61).

	TB		DFT/LDA		Exp.
	$V_{\rm eq}$	$V_{\rm exp}$	PP	LAPW $V_{\rm eq}$	
B	66.6	57.7	72	77.9	76.8
$c_{11}-c_{12}$	115.7	112.2	85	75.3	82.1
c_{11}	143.7	132.5	130	128.1	131.5
c_{12}	28.0	20.3	45	52.8	49.4
c_{44}^0	138.6	131.8	77		
c_{44}	111.9	107.2	63		68.4

TABLE III. Equilibrium total energies (eV/atom relative to the diamond structure energy) and unit-cell volumes (in units of the diamond structure equilibrium volume) and c/a ratios for some bulk phases of Ge computed with the TB model, compared with our LAPW DFT/LDA calculations (h-DIA, sc, sh, fcc, bcc) and literature values computed using DFT/LDA (two significantly different values have been published for the bc8 structure, as discussed in the text). For the body-centered-tetragonal 5-atom (bct-5) and the hexagonal-close-packed (hcp) structures no first-principles calculations were available. Structures used in the fitting database are labeled with an asterisk.

	TB			DFT/LDA		
Structure	E	V	c/a	E	V	c/a
h-DIA	0.003	0.993	1.64	0.017	0.994	1.65
sc*	0.175	0.836		0.213	0.840	
sh	0.189	0.834	0.95	0.168	0.805	0.94
β-Sn[a]	0.216	0.822	0.535	0.182	0.822	0.547
fcc*	0.224	0.809		0.260	0.812	
bc8[b]	0.231	0.916		0.125,0.033	0.915,0.881	
bct-5	0.279	0.912	1.81			
bcc*	0.283	0.790		0.302	0.814	
hcp	0.306	0.928	0.794			

[a]LDA from Ref. 58.
[b]LDA from Refs. 28 and 29.

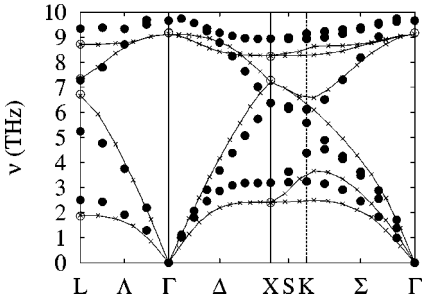

FIG. 4. Phonon frequencies for Ge computed with the sp^3 TB model (solid symbols) compared with DFT/LDA results (open symbols) from Ref. 63 and experimental results at 80 K from Ref. 64 (lines).

reasonable. We list the tested structures, as well as previously published results with other TB models[3,5,6] and first-principles results,[3,39] in Table VII.

The Ge_7 cluster is stable in the previously presented D_{5h} symmetry pentagonal bipyramid structure. There is less consensus on the ground-state structure of the Ge_8 cluster. We tested the edge capped pentagonal bipyramid [labeled C_s (1)],[3,39] the distorted octahedron face capped on two adjacent faces with C_2 symmetry,[3,39] the face capped pentagonal bipyramid [labeled C_s (2)],[3,5,6] and the C_{2h} symmetry distorted octahedron capped on two diametrically opposed faces.[39] We obtain the edge capped bipyramid as the ground state, essentially degenerate with the octahedron capped on adjacent faces. This result is consistent with the TB model of Zhao *et al.*[6] and the DFT/LDA work of Lu *et al.*,[39] although it conflicts with the AIMPRO first-principles code results of Sitch *et al.*[3]

A large number of structures have been proposed for the Ge_9 cluster, most in a C_{2v} symmetry. They comprise the distorted tricapped octahedron [C_{2v} (1)],[3,39] the distorted tricapped trigonal prism [C_{2v} (2)],[3] the capped tetragonal antiprism [C_{2v} (3)], the pentagonal bipyramid capped on adjacent faces (C_s),[5,6] and the capped distorted tetragonal prism [C_{2v} (4)].[6,39] Since first-principles calculations were available for only a few of these structures, we used the ABINIT plane-wave pseudopotential DFT/LDA code to compare on equal footing these five structures. We used a Troullier-Martins nonlocal pseudopotential, a plane-wave energy cutoff of 20 Ry, a cubic periodic supercell 11.2 Å on a side, and sampled the BZ at a single k point with reciprocal-lattice coordinates of $\frac{1}{4}\frac{1}{4}\frac{1}{4}$. We get two nearly degenerate ground-state structures, the distorted tricapped octahedron and the bicapped pentagonal bipyramid. While this is not in agreement with the DFT/LDA calculations, it is an error comparable to the work of Zhao *et al.* who specifically tailor their TB model for cluster properties.

TABLE V. Point defect formation energies (unrelaxed E_f^0 and relaxed E_f) computed with the TB model, and DFT/LDA calculations from Refs. 32 and 62.

	E_f^0	E_f	DFT E_f
V	4.6	3.6	1.9
I_t	3.1	2.5	3.2
I_h	5.6	4.4	2.9
$I_{\langle 110\rangle}$	4.3	3.3	2.3

TABLE VI. Surface energies (in eV/1×1 cell) and geometries for the Ge TB model, the Ge TB model with charge self-consistency (CSC), and DFT/LDA calculations. DFT calculations for (100) surface from Refs. 33,35–37, and (111) surface from Ref. 34. For the (100) surface, the x direction is parallel to the dimer bond, and for the (110) surface the x direction is normal to the surface bond zigzag rows.

	TB	TB-CSC	DFT/LDA
(100)			
$E(1\times1)$	1.93	2.31	
$\sigma_{xx}(1\times1)$	2.65	−0.03	
$\sigma_{yy}(1\times1)$	2.65	−0.03	
$E(2\times1)$ flat–$E(1\times1)$	−0.37	−0.69	−0.45 to −0.68
$\sigma_{xx}(2\times1)$ flat	0.39	0.42	
$\sigma_{yy}(2\times1)$ flat	−0.60	−0.27	
$E(2\times1)$ buckled−flat	−0.31	−0.30	−0.12 to −0.17
$\sigma_{xx}(2\times1)$ buckled	0.76	0.81	
$\sigma_{yy}(2\times1)$ buckled	−0.23	−0.23	
2×1 buckled r (Å)	2.60	2.56	2.48–2.54
2×1 buckled θ (°)	19.5	18.44	13–19
(111)			
$E(1\times1)$	1.51	1.55	1.40
$\sigma_{ii}(1\times1)$	−0.35	−0.32	−0.73
$E(2\times2)$ T_4	1.11	1.17	1.20
$\sigma_{ii}(2\times2)$ T_4	0.64	0.68	1.43
$E(2\times2)$ H_3	1.20	1.26	
$\sigma_{ii}(2\times2)$ H_3	0.34	0.39	
$E(2\times2)$ B_2	1.34	1.39	
(110)			
$E(1\times1)$	2.73	3.18	
$\sigma_{xx}(1\times1)$	−7.11	0.19	
$\sigma_{yy}(1\times1)$	−1.93	−1.03	

For the Ge_{10} cluster we considered three structures, the tetracapped trigonal prism with symmetry C_{3v},[5,6,39] the bicapped square antiprism with D_{4d} symmetry,[3,6] and the tetracapped octahedron with T_d symmetry.[3] We get nearly degenerate energies for the tetracapped trigonal prism and the bicapped square antiprism structures, with the tetracapped octahedron slightly higher in energy. This is a different ground state than either of the two predicted by the first-principles calculations, but quite similar to the TB model of Sitch *et al.*

Overall, the results of our sp^3 TB model for clusters are reasonable, although not perfect. It is inaccurate below seven atoms, but in the seven to ten atom range it is as good as other TB parametrizations available in the literature. This is despite the use of only bulk structures in our fitting database. For larger clusters, which have a more bulklike structure, we expect that our TB model will be even more accurate. In addition, previous experience with the fitting of parameters for the NRL-TB method suggests that refitting with a data-

TABLE VII. Symmetries and cohesive energies (in eV/atom) of Ge clusters with seven to ten atoms, computed by our TB model (NRL-TB), three other TB models (the work of Menon from Ref. 5, labelled MTB, the work of Zhao *et al.* from Ref. 6, labelled ZTB, and the density-functional TB work from Ref. 3, labelled DFTB) and three first-principles calculations (AIMPRO, DFT/LDA). Negative numbers indicate cohesive energy relative to lowest energy structure found by the same method.

	Sym.	NRL-TB[a]	MTB[b]	ZTB[c]	AIMPRO[d]	DFTB[e]	LDA[f]	LDA[g]
Ge_7	D_{5h}	2.91	3.19	3.09	−0.000	−0.000		
Ge_8	C_s (1)	2.87	3.17	3.05	−0.010	−0.003	3.685	
Ge_8	C_2	2.87			−0.036	−0.000	−0.003	
Ge_8	C_s (2)	2.82			−0.000	−0.056	−0.004	
Ge_8	C_{2h}	2.73		−0.08			−0.004	
Ge_9	C_{2v} (1)	3.03			−0.156	−0.167	−0.009	−0.000
Ge_9	C_{2v} (2)	2.84			−0.000	−0.000		−0.058
Ge_9	C_{2v} (3)	2.79						−0.091
Ge_9	C_s	3.03	3.25	3.12				−0.000
Ge_9	C_{2v} (4)	2.92		−0.06			3.791	−0.000
Ge_{10}	C_{3v}	3.08	3.32	3.17			+0.000	
Ge_{10}	D_{4d}	3.09		−0.16	−0.030	−0.000		
Ge_{10}	T_d	2.95			−0.000	−0.166		

[a]Present work.
[b]From Ref. 5.
[c]From Ref. 6.
[d]From Ref. 3.
[e]From Ref. 3.
[f]From Ref. 39.
[g]Present work.

base that emphasizes cluster properties could yield improved accuracy for clusters.[40–42]

VII. FINITE TEMPERATURE PROPERTIES

All of the properties discussed so far are related to energetics and structures at zero temperature, or to infinitesimal displacement from these geometries (e.g., the phonons and elastic constants). Such properties can be computed using at the most a few tens of force evaluations of a unit cell of about two hundred atoms. The computational efficiency of the TB model allows us to exceed the limitations of standard DFT by easily performing molecular-dynamics (MD) simulations that provide us with information about finite temperature properties.[43] As an example, we compute the mean-squared displacements of the atoms and the coefficient of thermal expansion for the diamond lattice as a function of applied temperature.

We perform a series of MD simulations using a diamond structure 686 atom unit cell, a $7\times7\times7$ supercell of the 2 atom fcc primitive unit cell, at temperatures ranging from 100 K to 2000 K, using 2-fs time steps. To set the temperature we initialize the velocities of the atoms to values selected randomly from a Boltzmann distribution consistent with twice the desired temperature, and perform a constant energy constant volume simulation. After about 200 time steps for equilibration, the temperature stabilizes at half the initial value (due to the equipartition theorem half of the initial energy, which was all kinetic, is converted into potential energy). We then track the atomic trajectories for 1800 time steps, and compute the mean-squared deviation of the atomic position averaging over all atoms and time steps. This mean-squared displacement is plotted in Fig. 5, together with experimental data derived from Debye-Waller factor measurement.[44] The TB model results have a slope that is about 35% smaller than experiment. At higher temperature the anharmonicity of the potential allows for larger mean-squared displacements than a simple linear extrapolation would predict.

The nearly linear dependence of the mean-squared displacement on temperature up to 2000 K indicates that even at this high temperature, the solid has not melted. While this temperature is significantly above the experimental melting point, this amount of overheating is not unusual for a simulation of a perfect periodic solid.[45] Nevertheless, the mean-squared displacement can be related to the melting point

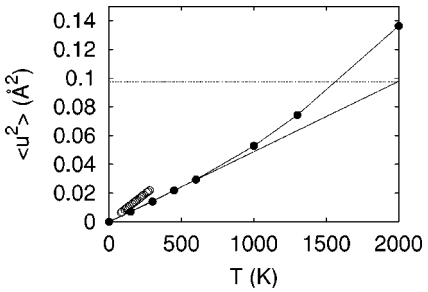

FIG. 5. Mean-squared displacement during MD simulation as a function of temperature. Solid symbols are MD simulation using the TB model, the line is a fit through the low temperature (up to 600 K) data, and open symbols are experimental data from Debye-Waller factor measurements (Ref. 44). The horizontal line indicates a mean-squared displacement of 0.13 times the bond length, squared.

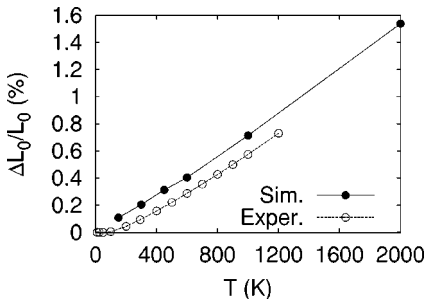

FIG. 6. Linear thermal expansion during MD simulation as a function of temperature. Solid symbols are MD simulation using the TB model, and open symbols are experimental data (Ref. 50).

through the Lindemann criterion, which states that the solid will melt when the root-mean-squared displacement is approximately 13% of the bond length.[46] This point is indicated by a horizontal line in Fig. 5. This value corresponds to a temperature of about 1560 K, somewhat above the experimental melting point of 1210 K.[47] In contrast, extrapolating a linear fit through the low-temperature results predicts the melting point at about 1990 K. This discrepancy highlights the need to include the full anharmonicity of the interatomic interactions when considering finite temperature properties.

Another finite temperature property that can be computed easily using a molecular-dynamics simulation based on TB forces is the thermal-expansion coefficient. We have computed this property using the same trajectories from the simulations of the atomic vibrations discussed above. During each trajectory we compute the mean pressure in the sample by averaging the values of the pressure (including both the kinetic and potential components[48,49]) sampled every 100 time steps (after the initial 100 time steps of equilibration). From the tabulated values of pressure as a function of temperature at constant volume we compute the equilibrium volume at each temperature. In this calculation we assume that the deviation from the equilibrium volume is small, so that the sample is in the harmonic regime. With this approximation, the difference between the simulation volume and the finite temperature equilibrium volume is

$$\Delta V(T) \approx V_0 \frac{P(T)}{B(T)},$$

where V_0 is the zero-temperature volume, $P(T)$ is the pressure at temperature T, and B is the bulk modulus. Since the volume differences are small and the volume scales as the cube of the length, the corresponding linear thermal expansion is

$$\frac{\Delta L(T)}{L_0} \approx \frac{1}{3} \frac{\Delta V(T)}{V_0}.$$

While we have calculated the bulk modulus at $T=0$, to compute the thermal expansion we also need at least an estimate of the variation of the bulk modulus with T. To determine this variation we computed the pressure at 1000 K in a system with a 3.1% lower volume. A pressure difference between the two volumes of 1.93 GPa indicates that the bulk modulus at this pressure is 62.3 GPa, 6.5% lower than the $T=0$ value of 66.6 GPa. Using the values of B at 0 K and 1000 K we assume a linear variation of B with T. With this approximation for $B(T)$ we compute the thermal expansion, plotted in Fig. 6, along with experimental data.[50] The transition in the experimental results from a linear T dependence at high T to a higher-order dependence at low T is caused by the increasing importance of the quantum-mechanical nature of phonons at low T.[51] Since MD describes the nuclei as classical point masses, a comparison with experiment is only meaningful at temperatures above the Debye temperature $\Theta_D = 360$ K.[52] In this range the agreement between the slopes of the experimental and simulated curves is very good. Using a linear least-squares fit, the slope of the experimental data is 7.15×10^{-4}%/K, while the slope of the simulation results is 7.34×10^{-4}%/K, a deviation of only 3%.

VIII. TWIST GRAIN BOUNDARY PROPERTIES

The most technologically important use for semiconductor materials is in the production of electronic devices, where material defects can have significant effects. While point defects (vacancies and interstitials) and line defects (dislocations) have been studied extensively using atomistic simulations with quantum-mechanical force calculations, grain boundaries (GB), a type of planar defect, have not. There have been a few simulations using both first-principles and tight-binding methods, but these have all been limited by the large system sizes and structural complexity inherent to the GB geometry. A number of studies of a particular high angle Ge twist GB have been performed using DFT/LDA,[53–56] but because of the computational demands of the method they were limited to a coarse exploration of the configuration space. In their examination of the $\Sigma = 5(001)$ twist GB their main conclusions were that a number of low-energy structures exist for the boundary, all of which include some atoms with coordination other than four, and that these broken bonds create defect states deep in the gap. In contrast, a related study of a $\Sigma = 5(310)$ tilt GB in silicon using a semiempirical TB model found only shallow states in the gap near the valence- and conduction-band edges.[57] In that TB study the absence of states deep in the gap, which was attributed to the perfect fourfold coordination of the atoms in the boundary, was used to support the idea that GB electrical activity is not intrinsic, but is instead related to GB defects or impurities.

In this section we present our study of the same high angle twist GB previously studied in the DFT/LDA work mentioned above, using a combination of the two TB models presented earlier. We use the sp^3 model, optimized for total-energy calculations, to systematically explore configuration space and compute relaxed geometries and energies. We then use the sp^3d^5 model, optimized for band-structure properties, to examine the band structure of the relaxed GB structures. We use the same basic geometry used in Ref. 56, with an in-plane unit cell determined by the coincident site lattice (CSL) unit cell, a $\sqrt{5} \times \sqrt{5}$ supercell of the fundamental (100) surface 1×1 unit cell. The calculation is carried out in a 70 atom supercell consisting of two grains, one with six

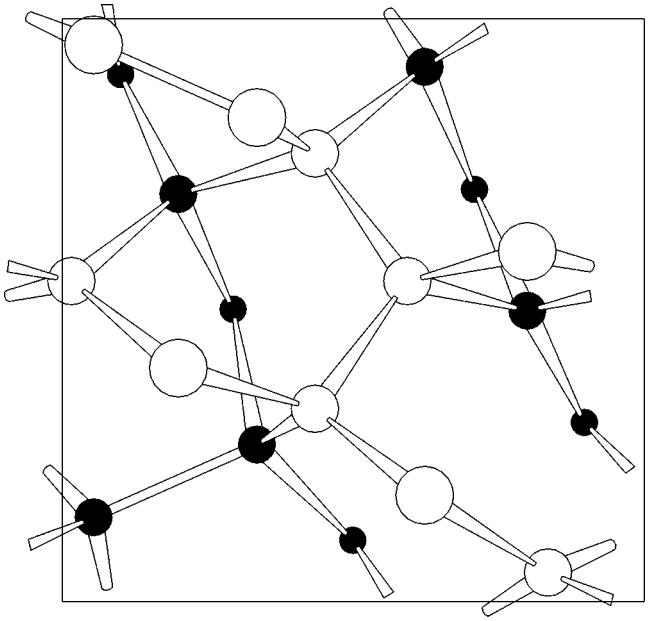

FIG. 7. Visualization of the lowest energy grain-boundary (GB) structure, showing features such as surface dimers but no coordination defects despite the low symmetry of the GB. View is along the (001) direction, atom color indicates the two grains, and size indicates distance along viewing direction. The square indicates the CSL unit cell.

layers and one with eight layers, with five atoms in each layer, with two special integration points in the Brillouin zone.

We sample the configuration space by generating a large number of initial GB geometries in the displacement site complete (DSC) unit cell. Since the TB approach is not as computationally demanding as DFT/LDA, we generate a 20 $\times 10$ mesh in the DSC cell, a much denser sampling than the 4×4 sampling used in Ref. 55. Each configuration is then relaxed with respect to atomic positions and unit-cell size normal to the interface in a four step process. We begin by generating a GB with the correct relative angle and in-plane displacement between the two grains, and some excess interlayer spacing at the GB relative to the bulk value. This is needed to prevent atoms from coming closer together than the distances sampled in the fit of the TB model, a situation that would correspond to unphysically high energies in any case. The initial GB is relaxed by applying uniaxial pressure to the sample normal to the GB, and keeping each five atom layer rigid but allowing it to move perpendicular to the GB. Further relaxation is achieved at zero applied pressure with constraints on two bilayers in the middle of each grain that allows them to move rigidly normal to the interface. In the final relaxation step the central bilayers are constrained to translate rigidly both normal to and in plane.

The qualitative results are similar to the DFT/LDA calculations. The GB energies range from 6.44 to 8.01 eV/CSL unit cell. These energies are comparable to the DFT/LDA results where the GB energies range from 5.79 to 7.04 eV/CSL unit cell. The denser mesh of initial configuration in the DSC unit cell generates a larger number of distinct minima than the seven considered by Tarnow *et al.*, fifteen in all. The

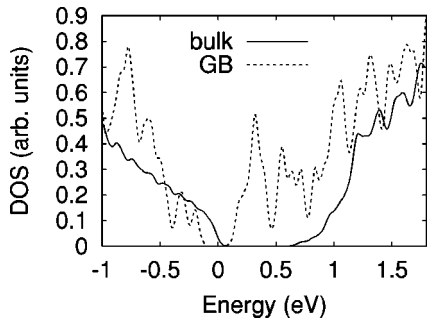

FIG. 8. Electronic density of states for the lowest energy GB structure (dashed line), and bulk diamond structure Ge calculated using the sp^3d^5 TB model. Energies are measured relative to the bulk conduction-band maximum.

lowest energy configuration, at (0.1,0.0) of the CSL lattice cell, is shown in Fig. 7 The same geometrical features seen in the DFT simulations, primarily free-surface-like intralayer dimers, dominate the relaxed GB structures. While this is not the same initial translation that led to the lowest energy structure in the work of Tarnow *et al.*, the difference is unlikely to be significant. We use a slightly different relaxation procedure, and the complex topology of the potential-energy surface means that even tiny differences in computed forces can lead the relaxation algorithm to a different minimum.

From the trough in the pair-correlation function we can define a distance cutoff for nearest neighbors at about 3.0 Å. Using this cutoff we have characterized the coordination statistics of each of the fifteen local minima. In the lowest energy configuration, as well as three other configurations with significantly higher energies (0.86 to 1.13 eV/CSL unit cell), all atoms are fourfold coordinated. The existence of such a structure with no coordination defects is unexpected considering the low symmetry of the GB structure. The other configurations range from two to four miscoordinated atoms, mainly threefold, but a few fivefold as well. It is interesting that the absence of coordination defects is not well correlated with a low GB energy.

One of the important properties of GB's, the nature of the electronic states associated with them, has been attributed to the presence or absence of coordination defects in the structure. For example, the TB simulation of the $\Sigma=5(310)$ tilt GB with perfectly fourfold coordinated atoms shows only shallow states,[57] while the DFT/LDA simulation of the $\Sigma=5(100)$ twist GB has coordination defects and deep states.[55] To examine the correlation between structure and gap states, we have calculated the electronic density of states (DOS) using a BZ sampling of 32 special k points (a $4\times 4\times 2$ mesh in the full BZ) and Gaussian broadening of 0.02 eV. We find that all of the relaxed GB structures have significant densities of states deep in the gap. In Fig. 8 we plot the DOS of the lowest energy GB structure, where all atoms are fourfold coordinated. The gap, which extends from about 0.0 to 0.65 eV, is clearly seen in the bulk diamond lattice DOS. In the GB sample there are states throughout that energy range. This indicates that even with a perfectly connected bond network defect states can exist deep in the gap.

IX. SUMMARY

We have developed two TB model parametrizations for germanium using the NRL-TB approach, one optimized for total-energy calculations and one for electronic structure calculations. The total-energy optimized model, which was fitted to energies and band structures of a few high-symmetry lattice structures, is transferable to a wide range of geometries. It has been tested for the energetics of other bulk structures, elastic constants and phonons, point defects, and surface properties, and in nearly every case gives very good agreement with first-principles calculations. These calculations include some properties that have not been simulated before using a quantum-mechanical method, including surface stresses for several (100) and (111) reconstructions, and the energies of the H_3 and B_2 2×2 adatom reconstruction of the (111) surface and the unreconstructed (110) surface. We have found that the addition of charge self-consistency terms to the Hamiltonian make negligible difference to the results for the bulk and point defect properties, but can strongly affect surface properties. In particular, the (110) surface geometry and stress are completely changed by the addition of charge self-consistency.

The TB model shows good transferability to intermediate size clusters, where the geometries are very different from the fitting database and none of the atoms are in bulklike environments. While structures and energies of clusters with fewer than seven atoms are not predicted accurately, between seven and ten atoms our sp^3 TB model shows very good agreement with other published calculations. These include both first-principles simulations, where available, and other TB models including some that were explicitly designed to reproduce cluster energetics.

Taking advantage of the efficiency of the TB approach, we have performed molecular-dynamics simulations using TB forces to compute some finite temperature properties that would be impractical to compute with first-principles approaches. We find good agreement with experiment for the atomic mean-squared displacement as a function of temperature, as well as the melting point estimated from this quantity using the Lindemann criterion. We also get a thermal-expansion coefficient in good agreement with experiment.

Finally, we take advantage of the transferability of the TB models to a wide range of geometries combined with their ability to give electronic structure information to study a high angle twist grain boundary. We get qualitative agreement with previous DFT/LDA calculations in the energetics of the grain-boundary structure, and we find a fully fourfold coordinated minimum-energy structure. For all of the stable structures we find electronic states in midgap, which would lead to electrical activity for this type of boundary. This stands in contrast to previous TB modeling of high angle twist boundaries, where the fully fourfold coordinated structure created only shallow states near the band edges.

ACKNOWLEDGMENTS

This work was supported by the United States Office of Naval Research and the Common High Performance Computing Software Support Initiative (CHSSI) of the United States Department of Defense High Performance Computing Modernization Program (HPCMP). The authors would like to thank Dr. Steve Erwin for valuable discussions. The pseudopotential plane-wave DFT/LDA results were obtained using the ABINIT code, a common project of the Universite Catholique de Louvain, Corning Incorporated, and other contributors (URL http://www.pcpm.ucl.ac.be/abinit).

[1] *Tight-Binding Approach to Computational Materials Science*, edited by P. E. A. Turchi, A. Gonis, and L. Colombo, MRS Symposia Proceedings No. 49 (Materials Research Society, Warrendale, 1998).
[2] J. L. Mercer, Jr. and M. Y. Chou, Phys. Rev. B **47**, 9366 (1993).
[3] P. K. Sitch, T. Frauenheim, and R. Jones, J. Phys.: Condens. Matter **8**, 6873 (1996).
[4] S. K. Mishra and S. Satpathy, Physica B **254**, 234 (1998).
[5] M. Menon, J. Phys.: Condens. Matter **10**, 10 991 (1998).
[6] J. Zhao, J. Wang, and G. Wang, Phys. Lett. A **275**, 281 (2000).
[7] D. J. Chadi and M. L. Cohen, Phys. Status Solidi B **68**, 405 (1975).
[8] P. Vogl, H. P. Hjalmarson, and J. D. Dow, J. Phys. Chem. Solids **44**, 365 (1983).
[9] D. A. Papaconstantopoulos, in *Handbook of the Band Structure of Elemental Solids* (Plenum Press, New York, 1986), Chap. 1.
[10] G. Grosso and C. Piermarocchi, Phys. Rev. B **51**, 16772 (1995).
[11] M. J. Mehl and D. A. Papaconstantopoulos, Phys. Rev. B **54**, 4519 (1996).
[12] N. Bernstein, M. J. Mehl, D. A. Papaconstantopoulos, N. I. Papanicolaou, M. Z. Bazant, and E. Kaxiras, Phys. Rev. B **62**, 4477 (2000).
[13] M. Elstner, D. Porezag, G. Jungnickel, J. Elsner, M. Haugk, T. Frauenheim, S. Suhai, and G. Seifert, Phys. Rev. B **58**, 7260 (1998).
[14] D. A. Papaconstantopoulos, M. J. Mehl, S. C. Erwin, and M. R. Pederson, in *Tight-Binding Approach to Computational Materials Science* (Ref. 1), pp. 221–230.
[15] O. K. Andersen, Phys. Rev. B **12**, 3060 (1975).
[16] S.-H. Wei and H. Krakauer, Phys. Rev. Lett. **55**, 1200 (1985).
[17] D. Singh, Phys. Rev. B **43**, 6388 (1991).
[18] D. J. Singh, *Planewaves, Pseudopotentials, and the LAPW Method* (Kluwer Academic, Boston, 1994).
[19] D. A. Papaconstantopoulos, Phys. Rev. B **27**, 2569 (1983).
[20] G. A. Baraff and M. Schluter, Phys. Rev. B **30**, 3460 (1984).
[21] V. Fiorentini and A. Baldereschi, Phys. Rev. B **51**, 17 196 (1995).
[22] R. E. Cohen, M. J. Mehl, and D. A. Papaconstantopoulos, Phys. Rev. B **50**, 14 694 (1994).
[23] M. J. Mehl and D. A. Papaconstantopoulos, in *Topics in Computational Materials Science*, edited by C. Y. Fong (World Scientific, Singapore, 1998).
[24] The parameters are available in a computationally accessible form at http://cst-www.nrl.navy.mil/bind/ge.html

[25] I. Shavitt, in *Methods in Computational Physics*, edited by B. Alder, S. Fernbach, and M. Rotenberg (Academic Press, New York, 1963), Vol. 2, pp. 1–45.
[26] C. Herring, in *Fundamental Formulas of Physics*, edited by D. H. Menzel (Dover, New York, 1960), Vol. 2, p. 599.
[27] D. D. Johnson, Phys. Rev. B **38**, 12 807 (1988).
[28] A. Mujica and R. J. Needs, Phys. Rev. B **48**, 17 010 (1993).
[29] J. Crain, R. O. Piltzo, G. S. Ackland, S. J. Clark, M. C. Payne, V. Milman, J. S. Lin, P. D. Hatton, and Y. H. Nam, Phys. Rev. B **50**, 8389 (1994).
[30] M. J. Mehl, B. M. Klein, and D. A. Papaconstantopoulos, in *Intermetallic Compounds*, edited by J. H. Westbrook and R. L. Fleischer (Wiley, New York, 1994), Vol. 1, Chap. 9.
[31] K.-M. Ho, C. L. Fu, B. N. Harmon, W. Weber, and D. R. Hamann, Phys. Rev. Lett. **49**, 673 (1982).
[32] A. J. R. da Silva, A. Janotti, A. Fazzio, R. J. Baierle, and R. Mota, Phys. Rev. B **62**, 9903 (2000).
[33] M. Needels, M. C. Payne, and J. D. Joannopoulos, Phys. Rev. Lett. **58**, 1765 (1987).
[34] R. D. Meade and D. Vanderbilt, Phys. Rev. B **40**, 3905 (1989).
[35] L. Spiess, A. J. Freeman, and P. Soukiassian, Phys. Rev. B **50**, 2249 (1994).
[36] P. Kruger and J. Pollmann, Phys. Rev. Lett. **74**, 1155 (1995).
[37] C. Yang and H. C. Kang, J. Chem. Phys. **110**, 11 029 (1999).
[38] H. Balamane, T. Halicioglu, and W. A. Tiller, Phys. Rev. B **46**, 2250 (1992), see also references therein.
[39] Z.-Y. Lu, C.-Z. Wang, and K.-M. Ho, Phys. Rev. B **61**, 2329 (2000).
[40] Y. Xie and J. A. Blackman, Phys. Rev. B **63**, 125105 (2001).
[41] C. Barreteau, D. Spanjaard, and M. C. Desjonqueres, Phys. Rev. B **58**, 9721 (1998).
[42] C. Barreteau, R. Guirado Lopez, D. Spanjaard, M. C. Desjonqueres, and A. M. Oles, Phys. Rev. B **61**, 7781 (2000).
[43] F. Kirchhoff, M. J. Mehl, N. I. Papanicolaou, D. A. Papaconstantopoulos, and F. S. Kahn, Phys. Rev. B **63**, 195101 (2001).
[44] L. M. Peng, G. Ren, S. L. Dudarev, and M. J. Whelan, Acta Crystallogr., Sect. A: Found. Crystallogr. **A52**, 456 (1996).
[45] D. Wolf, P. R. Okamoto, S. Yip, J. F. Lutsko, and M. Kluge, J. Mater. Res. **5**, 286 (1990).
[46] F. A. Lindemann, Phys. Z **11**, 609 (1910).
[47] R. C. Weast, *CRC Handbook of Chemistry and Physics*, edited by M. J. Astle and W. H. Beyer (CRC Press, Boca Raton, 1986), pp. B–18.
[48] M. P. Allen and D. J. Tildesley, in *Computer Simulations of Liquids* (Oxford University Press, Oxford, 1987), p. 78.
[49] E. B. Tadmor, G. S. Smith, N. Bernstein, and E. Kaxiras, Phys. Rev. B **59**, 235 (1999).
[50] *Thermophysical Properties of Matter*, edited by Y. S. Touloukian, R. K. Kirby, R. E. Taylor, and P. D. Desai (IFI/Plenum, New York, 1975), Vol. 12, p. 116.
[51] R. K. Pathria, *Statistical Mechanics* (Pergamon Press, Oxford, 1991), pp. 197, 213.
[52] N. W. Ashcroft and N. D. Mermin, *Solid State Physics* (Saunders College, Philadelphia, 1976), p. 461.
[53] M. C. Payne, P. D. Bristowe, and J. D. Joannopoulos, Phys. Rev. Lett. **58**, 1348 (1987).
[54] E. Tarnow, P. D. Bristowe, J. D. Joannopoulos, and M. C. Payne, J. Phys.: Condens. Matter **1**, 327 (1989).
[55] E. Tarnow, P. Dallot, P. D. Bristowe, J. D. Joannopoulos, G. P. Francis, and M. C. Payne, Phys. Rev. B **42**, 3644 (1990).
[56] C. Molteni, G. P. Francis, M. C. Payne, and V. Heine, Phys. Rev. Lett. **76**, 1284 (1996).
[57] M. Kohyama, R. Yamamoto, Y. Ebata, and M. Kinoshita, J. Phys. C **21**, 3205 (1988).
[58] N. Moll, M. Bockstedte, M. Fuchs, E. Pehlke, and M. Scheffler, Phys. Rev. B **52**, 2550 (1995).
[59] O. H. Nielsen and R. M. Martin, Phys. Rev. B **32**, 3792 (1985).
[60] H. J. McSkimin, J. Appl. Phys. **24**, 988 (1953).
[61] H. J. McSkimin and J. P. Andreatch, J. Appl. Phys. **35**, 3312 (1964).
[62] A. Fazzio, A. Janotti, A. J. R. da Silva, and R. Mota, Phys. Rev. B **61**, R2401 (2000).
[63] P. Giannozzi, S. de Gironcoli, P. Pavone, and S. Baroni, Phys. Rev. B **43**, 7231 (1991).
[64] G. Nelin and G. Nilsson, Phys. Rev. B **5**, 3151 (1972).